Deterministic spin-orbit torque switching including the interplay between spin polarization and kagome plane in Mn_3Sn

Zhengde Xu [1,2,3] Xue Zhang,[1,2,3] Yixiao Qiao,[1] Gengchiau Liang,[4,5] Shuyuan Shi,[6,*] and Zhifeng Zhu [1,7,†]

[1]*School of Information Science and Technology, ShanghaiTech University, Shanghai 201210, China*
[2]*Shanghai Institute of Microsystem and Information Technology, Chinese Academy of Sciences, Shanghai 200050, China*
[3]*University of Chinese Academy of Sciences, Beijing 100049, China*
[4]*Department of Electrical and Computer Engineering, National University of Singapore, 117576 Singapore*
[5]*Industry Academia Innovation School, National Yang-Ming Chiao Tung University, Hsinchu City 300093, Taiwan*
[6]*Fert Beijing Institute, MIIT Key Laboratory of Spintronics, School of Integrated Circuit Science and Engineering, Beihang University, Beijing 100191, China*
[7]*Shanghai Engineering Research Center of Energy Efficient and Custom AI IC, Shanghai 201210, China*

(Received 29 August 2023; revised 11 March 2024; accepted 4 April 2024; published 23 April 2024)

Previous research has demonstrated the spin-orbit torque (SOT) switching of Mn_3Sn in configuration I, where the spin polarization $\boldsymbol{\sigma}$ resides within the kagome plane. However, this configuration has yielded several unexpected outcomes, giving rise to debates concerning the fundamental physics governing the switching process. Alternatively, in configuration II, $\boldsymbol{\sigma}$ is perpendicular to the kagome plane, which bears greater resemblance to the ferromagnetic system. In this study, we show successful SOT switching of Mn_3Sn in configuration II, demonstrating behaviors more akin to ferromagnets, e.g., the critical switching current density (J_{crit}) and external field (H_{ext}) are in the order of 10^{10} A/m^2 and tens of Oersted, respectively. The switching result is also independent of the initial state. We further show that the distinctive spin structure of Mn_3Sn leads to unique switching characteristics, including J_{crit} increasing linearly with H_{ext} and the opposite switching polarity to ferromagnetism. A switching phase diagram is further provided as a guideline for experimental demonstrations, offering a clear physical picture for the observed phenomena.

DOI: 10.1103/PhysRevB.109.134433

I. INTRODUCTION

The increasing demand for higher memory performance stimulates the research of magnetic random access memory (MRAM). In the last two decades, the development of current control of magnetic states in ferromagnets [1–3] enables fast switching in subnanoseconds [4], low switching current density of 10^9 A/m^2 [5], and small device in nanometer diameters [6]. To further improve the performance, in recent years people turned their attention to antiferromagnets which consist of antiparallelly aligned magnetic moments [7–10]. They can be roughly divided into collinear and noncollinear antiferromagnets. Compared to the widely studied collinear antiferromagnets [11–14], the spin-orbit torque (SOT) switching of noncollinear antiferromagnets remains to be explored.

Mn_3Sn is an exemplary material for the noncollinear antiferromagnets [15–20]. It has exotic properties such as the large anomalous Hall effect (AHE) [21]. This enables effective read out of the magnetic state. The SOT switching of Mn_3Sn was demonstrated in a bilayer Mn_3Sn/Heavy Metal (HM) structure, in which the spin polarization lies in the kagome plane (configuration I) [22–25]. The authors attribute the switching mechanism the same as ferromagnets. However, the high critical switching current density ($J_{crit} = 10^{14}$ A/m^2) required in the simulation does not match that in experiments, which has motivated further studies that attribute the much smaller J_{crit} from experiments to the indispensable role from the thermal effect [26,27]. In fact, there can be three configurations in the SOT switching of Mn_3Sn. As illustrated in Fig. 1(c), in configuration II, the spin polarization is perpendicular to the kagome plane, whereas in configuration III the kagome plane is parallel to the thin film. In configuration II, SOT induced magnetization oscillation has been observed [22,28–31]. By introducing magnetostriction, the spin configuration can be modified to sustain the perpendicular magnetic octupole, which can then be switched by SOT [17]. However, the switching in the normal Mn_3Sn system (i.e., where the spin configurations are not distorted) has not been reported. A recent study provided experimental evidence for this magnetization switching [32], but it was attributed to the misalignment of crystalline orientation and thus classified to configuration I. Intuitively, configuration II is more like the SOT switching of perpendicular ferromagnets since the spin polarization $\boldsymbol{\sigma}$ is orthogonal to all magnetic moments. Therefore, it is crucial to explore and understand the switching behaviors in configuration II.

In this work, we first provide a complete magnetization dynamics diagram for configuration I. Besides reproducing the large J_{crit} [22,26], we find the switching results are sensitive to the initial state. In addition, J_{crit} is independent of H_{ext} [22,26,32]. Configuration I is therefore very different from the ferromagnet switching. We then study the magnetization

*Corresponding author: smeshis@buaa.edu.cn
†Corresponding author: zhuzhf@shanghaitech.edu.cn

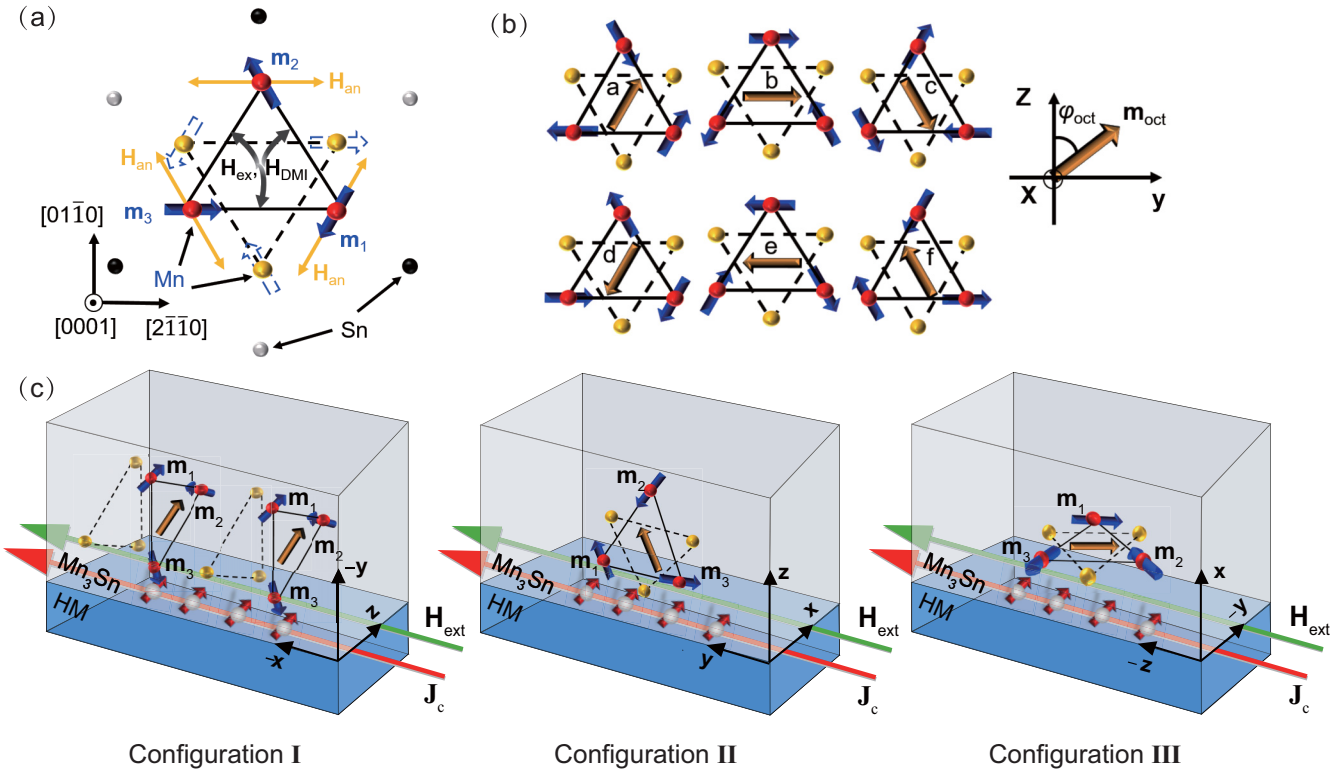

FIG. 1. (a) Atomic structure of Mn_3Sn. The red and yellow circles denote Mn atoms on the different layers. The black and silver circles denote Sn atoms on the same layer of yellow and red Mn, respectively. (b) The six equivalent states of Mn_3Sn, which are defined as states a, b, c, d, e, and f, respectively. The corresponding angles are $\varphi = 30°$, $90°$, $150°$, $210°$, $270°$, $330°$. (c) The three device configurations which are defined as configurations I, II, and III, respectively. In configuration I, the line connecting m_1 and m_3 points to $+\mathbf{y}$ direction.

dynamics in configuration II. We first reproduce the magnetization oscillation when $\mathbf{H}_{\text{ext}}$ is absent or small. Interestingly, further increase in $\mathbf{H}_{\text{ext}}$ leads to successful switching, with J_{crit} in the order of 10^{10} A/m^2 and H_{ext} of 100 Oe. In addition, we show J_{crit} varies with H_{ext}, and the switching result is independent of the initial state. These features are highly similar to ferromagnet switching. However, the complex spin structure in Mn_3Sn produces many distinct features, e.g., J_{crit} increases with H_{ext}, faster and with less precession switching compared with that in ferromagnets, and opposite switching polarities to ferromagnets. Finally, we provide a phase diagram to guide future experiment verification. Our work reveals the importance of considering the spin configuration in the noncollinear antiferromagnet switching. It also provides insights to better understand the magnetization dynamics in Mn_3Sn-like antiferromagnets.

II. METHODOLOGY

Mn_3Sn is studied using the three sublattice macrospin model. As shown in Fig. 1(a), the three sublattice are marked as red circles. The energy of this system is determined by the following Hamiltonian:

$$\mathbf{H} = A\sum_{i,j}\mathbf{m}_i\cdot\mathbf{m}_j + \sum_{i,j}\boldsymbol{D}_{ij}\cdot(\mathbf{m}_i\times\mathbf{m}_j) - \sum_i(\mathbf{K}_i\cdot\mathbf{m}_i)^2 - \mu_0 m_s\sum_i(\mathbf{m}_i\cdot\mathbf{H}_{\text{ext}}),$$

where the exchange interaction constant $A = 17.53$ meV, the Dzyaloshinskii-Moriya (DM) interaction $D = 0.833$ meV, the magnetic anisotropy constant $K = 0.196$ meV, and the magnetic moment $m_s = 3\mu_B$. All these parameters are the same as in Ref. [15]. We only consider the exchange and DM interaction between the nearest neighbors in the same layer [22,28,33]. The easy axis of crystalline anisotropy is marked by the yellow arrows, which point to the nearest Sn atoms. The last term is the Zeeman energy due to the external magnetic field $\mathbf{H}_{\text{ext}}$.

The dynamics of magnetic moments are described by the coupled Landau-Lifshitz-Gilbert-Slonczewski (LLGS) equations [34–36],

$$\frac{d\mathbf{m}_i}{dt} = -\gamma\mathbf{m}_i\times\mathbf{H}_{\text{eff},i} + \alpha\mathbf{m}_i\times\frac{d\mathbf{m}_i}{dt} - \gamma\frac{\hbar\theta_{\text{SH}}J_c}{2eM_s d}\mathbf{m}_i\times(\mathbf{m}_i\times\boldsymbol{\sigma}_i).$$

The first term on the right-hand side represents the precession of the magnetic moment around the effective magnetic field $\mathbf{H}_{\text{eff},i} = -\frac{1}{m_s}\frac{\partial\mathbf{H}}{\partial\mathbf{m}}$. The second term describes the Gilbert damping, and the last term is the SOT. γ is the gyromagnetic ratio, and $\alpha = 0.003$ [22] is the damping constant. The spin-Hall angle $\theta_{\text{SH}} = 0.06$ [17] and the thickness of the Mn_3Sn film $d = 30$ nm [17] are used in the simulation. The saturation magnetization M_s is calculated as $M_s = 6m_s/V_{\text{cell}}$ [22] with the unit cell volume $V_{\text{cell}} = 0.3778\,\text{nm}^3$. The coupled LLGS equations are numerically solved via the Runge-Kutta fourth-

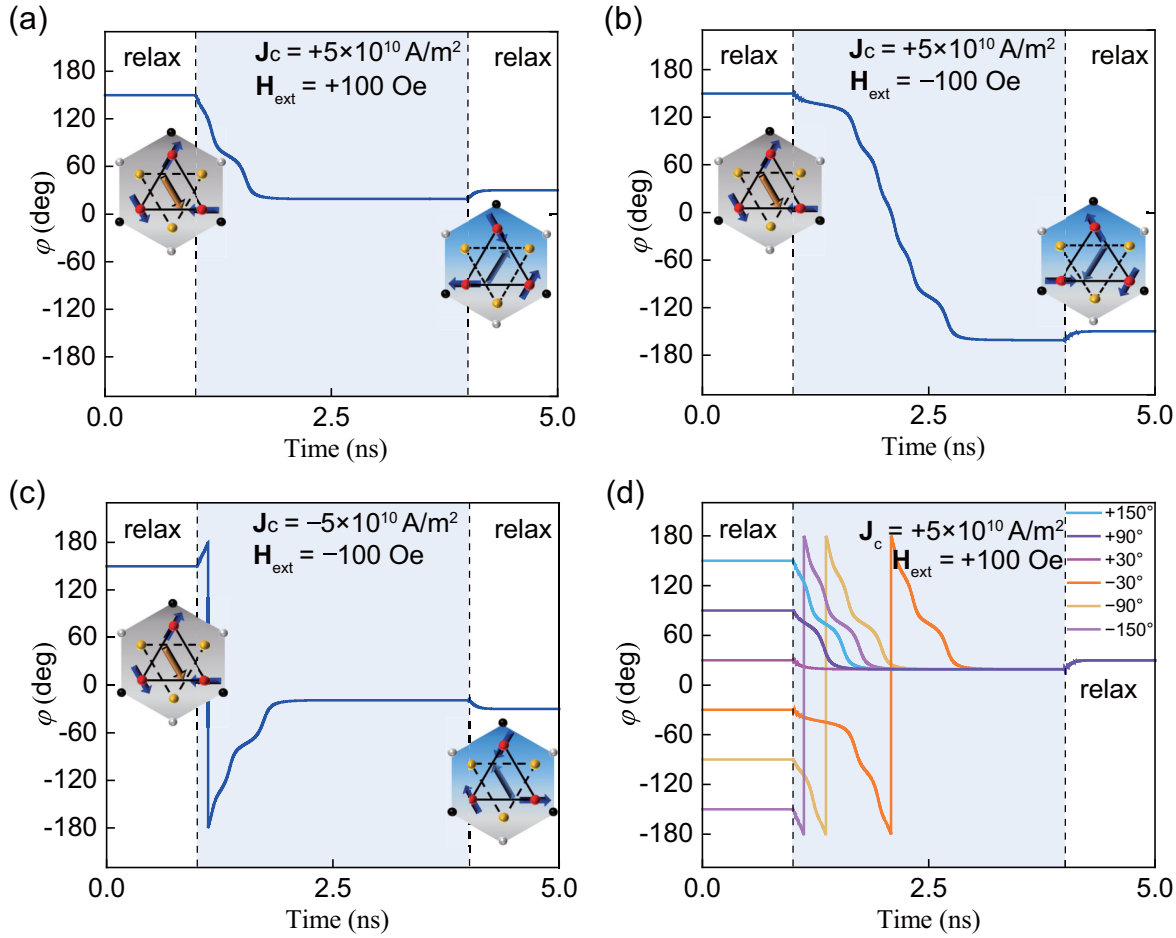

FIG. 2. The dynamics of octupole moment in configuration II. Before turning on $\mathbf{J}_c$ and $\mathbf{H}_{ext}$, the system is relaxed for 1 ns to reach the equilibrium state. At 4 ns, both $\mathbf{J}_c$ and $\mathbf{H}_{ext}$ are removed, and the system is relaxed to the new stable state. The insets show the spin structure for the initial and final states.

order method. The simulation time step is 5 fs. The relaxation of the system leads to a finite net magnetization comparable to that previously reported [22].

III. RESULTS AND DISCUSSION

In equilibrium, Mn_3Sn has six states that are equivalent in energy. As shown in Fig. 1(b), we define them as states a, b, c, d, e, and f, respectively. In the Mn_3Sn/HM bilayer, there can be three configurations where the kagome plane is perpendicular to any of the three orthogonal axes [22]. Previous studies have demonstrated SOT switching of Mn_3Sn in configuration I [22,26–28]. We have reproduced these results in Supplemental Material S1 [37], i.e., starting from state c, it can be switched to state d and vice versa [22,26]. Some studies claim the switching mechanism is the same as that in ferromagnets. However, J_{crit} required in simulation is very large (i.e., in the order of 10^{14} A/m^2 (see Fig. S1 [37] and Refs. [20,24]), inconsistent with experimental values. This discrepancy motivates recent studies that conclude the crucial role of thermal effects [26,27]. Besides the large current density required to switch Mn_3Sn in configuration I, one must notice other important differences compared to that in ferromagnets. Since the six states are equivalent, there will be a total of six switching cases when each stable state is used as the initial state. Previous studies only discussed two of them [22,26], i.e., starting from states c and d. We first complete all the switching cases. As shown in Table S1 of the Supplemental Material [37], states a and f can be reached by applying $\mathbf{J}_c$ and $\mathbf{H}_{ext}$, but states b and e will not be alerted. In addition, when $\mathbf{J}_c$ is along the $-\mathbf{x}$ direction and $\mathbf{H}_{ext}$ is along the $+\mathbf{x}$ direction, state a is switched to state f, but state c is switched to state d. This shows that under a fixed combination of $\mathbf{J}_c$ and $\mathbf{H}_{ext}$, the switching results are sensitive to the initial state. This is in stark contrast to the SOT switching of perpendicularly magnetized ferromagnets, in which the direction of switching is independent of the initial state, i.e., when both $\mathbf{J}_c$ and $\mathbf{H}_{ext}$ are fixed, the magnetization in ferromagnets will always favor one direction (either $+\mathbf{z}$ or $-\mathbf{z}$). In addition, it has been experimentally demonstrated that J_{crit} is independent of H_{ext} in configuration I [22,26,32], whereas J_{crit} decreases with H_{ext} in ferromagnet switching [38]. Most importantly, since $\boldsymbol{\sigma}$ lies in the kagome plane in configuration I, there will be collinear component between $\boldsymbol{\sigma}$ and magnetic moments, which is different from the switching of perpendicular ferromagnets where $\boldsymbol{\sigma}$ is perpendicular to the magnetization. In fact, configuration II is more like the ferromagnet system since $\boldsymbol{\sigma}$ is orthogonal to all magnetic moments. In addition, the

TABLE I. Switching cases in configuration II.

Initial state	$J_c = +y, H_{ext} = +y$	$J_c = -y, H_{ext} = -y$	$J_c = +y, H_{ext} = -y$	$J_c = -y, H_{ext} = +y$
a 30°	*a* 30°	*f* 330°	*d* 210°	*c* 150°
b 90°	*a* 30°	*f* 330°	*d* 210°	*c* 150°
c 150°	*a* 30°	*f* 330°	*d* 210°	*c* 150°
d 210°	*a* 30°	*f* 330°	*d* 210°	*c* 150°
e 270°	*a* 30°	*f* 330°	*d* 210°	*c* 150°
f 330°	*a* 30°	*f* 330°	*d* 210°	*c* 150°

corresponding effective SOT field lies in the kagome plane, resulting in an effective control of magnetization. Therefore, we expect that there will be magnetization switching in configuration II.

In configuration II, when $\mathbf{H}_{ext}$ is absent, the magnetic moments develop into oscillation [Fig. S2(a) of the Supplemental Material [37]], which has been demonstrated previously [28]. The case with $\mathbf{H}_{ext}$ applied along $\mathbf{J}_c$ has been studied before [22], where they predict oscillation instead of deterministic switching. As shown in Fig. S2(b) [37], under a small $\mathbf{H}_{ext} =$ 50 Oe, this oscillation has also been reproduced. However, when we apply $\mathbf{J}_c = 5\times10^{10}\,\mathrm{A/m^2}$ and $\mathbf{H}_{ext}$ is increased to 100 Oe along the $+\mathbf{y}$ direction, as shown in Fig. 2(a), deterministic switching is observed, i.e., state *c* is switched to state *a*. When $\mathbf{H}_{ext}$ is reversed, state *c* is switched to state *d* [see Fig. 2(b)]. When we further reverse $\mathbf{J}_c$, state *c* is switched to state *f* [see Fig. 2(c)]. These results demonstrate that both SOT and $\mathbf{H}_{ext}$ are indispensable in the switching of Mn_3Sn. In addition, J_{crit} is in the order of $10^{10}\,\mathrm{A/m^2}$. As shown in Fig. 2(d), we also verify that the switching direction only depends on the combination of $\mathbf{J}_c$ and $\mathbf{H}_{ext}$ and is independent of the initial state, e.g., regardless of the initial state, $\mathbf{J}_c$ and $\mathbf{H}_{ext}$ along the $+\mathbf{y}$ direction will always bring the system to state *a*. Both features are similar to ferromagnets. The complete switching cases are summarized in Table I. From the table, we notice that states *b* and *e* can never be reached, which happens to give zero AHE signal. We also notice that the switching process has less precession, which is a key feature of antiferromagnets that possess strong exchange coupling between sublattices, rather than being attributed to the neglected field-like torque (FLT) in the simulation (Supplemental Material S3 [37]). This also leads to ultrafast switching completed in subnanoseconds as shown in Fig. 2(a).

Since the magnetic moment in Mn_3Sn is more sensitive to the in-plane effective field [39], we propose to understand our switching results by analyzing the effective field that exerts on the magnetic octupole ($\mathbf{m}_{oct} = \frac{\mathbf{m}_1+\mathbf{m}_2+\mathbf{m}_3}{3}$). The effective field corresponding to the dampinglike torque acting on each magnetic moment is in the form $\mathbf{H}_{eff\_DLT} = \frac{\hbar\theta_{SH}J_c}{2eM_sd}\boldsymbol{\sigma}\times\mathbf{m}_{oct}$. As shown in Fig. 3(a), $\mathbf{J}_c$ in the $+\mathbf{y}$ direction gives $\boldsymbol{\sigma}$ along the $+\mathbf{x}$ direction, resulting in $\mathbf{H}_{eff\_DLT}$ shown as the blue arrow. $\mathbf{H}_{eff\_DLT}$ compensates for H_{ext} which points in the $+\mathbf{y}$ direction. Following this principle, the other three cases can be derived as shown in Figs. 3(b)–3(d). These results are consistent with those obtained from numerical simulations as shown in Table I. Now we can easily understand why states *b* and *e* can never be reached. Since $\mathbf{m}_{oct}$ in these two states points to 90° and 270°, the corresponding torque from $\mathbf{H}_{ext}$ vanishes. Therefore, the balance between effective fields cannot be achieved under a finite $\mathbf{J}_c$. These two states

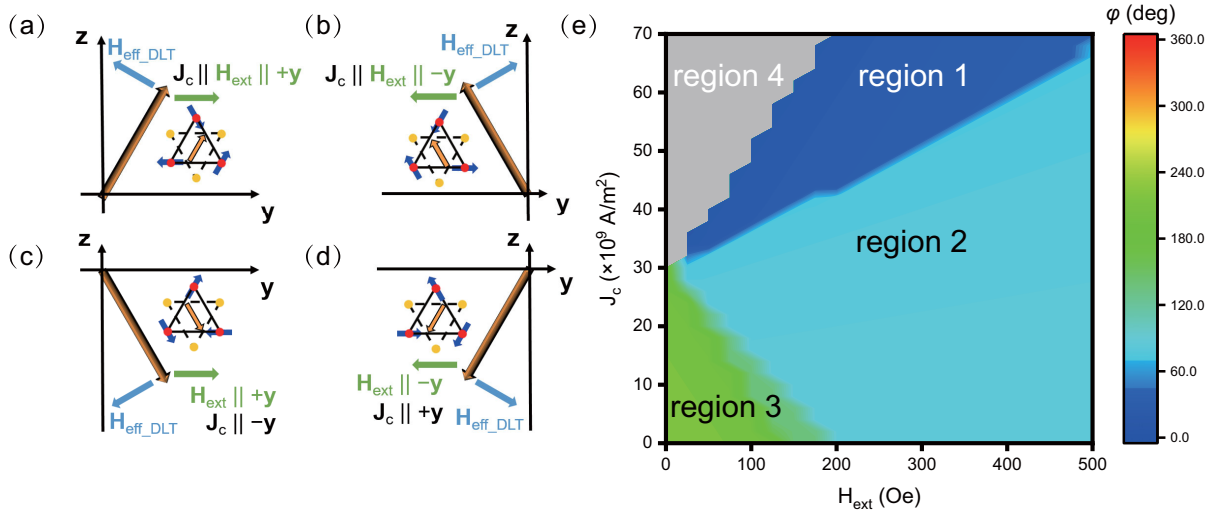

FIG. 3. (a)–(d) Illustration of effective fields from spin-orbit torque and external field. (e) The switching phase diagram when J_c and H_{ext} are varied. Region 1 denotes successful switching from state *d* to state *a*. The octupole moment aligns to $\mathbf{H}_{ext}$ in region 2. In region 3, the magnetic moments remain in the initial state. In region 4, the magnetic moments develop into oscillation.

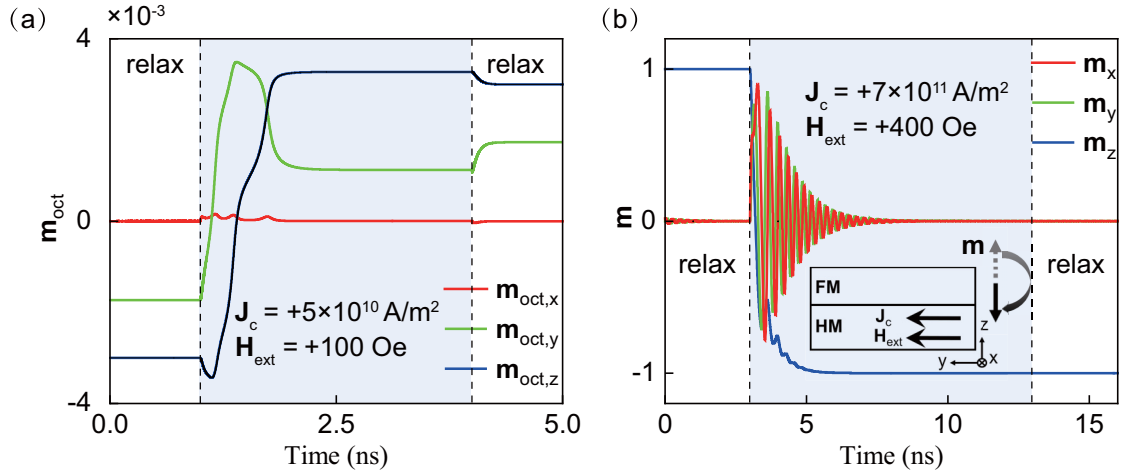

FIG. 4. Dynamics of the (a) octupole moment in Mn_3Sn and (b) magnetization in ferromagnets. Both devices have $\theta_{SH} > 0$. $\mathbf{J}_c$ and $\mathbf{H}_{ext}$ in both cases are along $+y$ direction.

will finally evolve into either of the four states shown in Figs. 3(a)–3(d).

Following this explanation, one expects that J_{crit} should become larger when H_{ext} is increased. This has been verified in the phase diagram shown in Fig. 3(e). In the phase diagram, the initial state is state d, and the successful switching to state a is denoted as region 1 using the blue color. As H_{ext} is increased from 25 to 500 Oe, J_{crit} increases linearly from 3.2×10^{10} to 7×10^{10} A/m^2. Notice that the strength of $\mathbf{H}_{eff\_DLT}$ is a linear function of J_c; the linear trend shown in the phase diagram again supports our explanation that the switching is realized by the balance of effective SOT field and the external field. In contrast, in the ferromagnet system, it is well known that J_{crit} becomes smaller when H_{ext} increases [38]. In fact, a similar qualitative explanation can be applied to ferromagnets [40], but it fails to justify the relation between J_{crit} and H_{ext}. In addition, in the ferromagnet system, even using the macrospin model, J_{crit} still decreases when H_{ext} becomes larger. This demonstrates the critical differences between the SOT switching in Mn_3Sn and in perpendicular ferromagnets.

Furthermore, we find the SOT-induced switching polarities are opposite between Mn_3Sn and ferromagnets. It has been shown in Fig. 2(d) that the octupole will be switched to state a with $\varphi = 30°$, i.e., the z component of the octupole moment ($m_{oct,z}$) is larger than 0. We redraw the dynamics of $\mathbf{m}_{oct}$ in Fig. 4(a). In comparison, we study the switching of perpendicular ferromagnets in the same setup, i.e., the device consists of a ferromagnet/HM bilayer where $\theta_{SH} > 0$. When both $\mathbf{J}_c$ and $\mathbf{H}_{ext}$ are applied in the $+\mathbf{y}$ direction, as shown in Fig. 4(b), the magnetic moment switches from $+\mathbf{z}$ to $-\mathbf{z}$. This comparison shows that despite the similar device configuration, the underlying switching mechanism is different between Mn_3Sn and ferromagnets.

To complete the switching diagram, we further increase H_{ext}. Under a fixed $J_c = 5\times10^{10}$ A/m^2, when H_{ext} is increased above 275 Oe, the octupole moment will align with the magnetic field, i.e., $\varphi = 90°$ [see Fig. 5(a)]. Note that there is an abrupt change in the magnetic state when H_{ext} exceeds the critical value (H_{crit}), dividing the phase diagram into two distinct regions, i.e., regions 1 and 2 in Fig. 3(e). As shown in Fig. 5(b), for $H_{ext} > H_{crit}$, the switching results are independent of the initial state. When $\mathbf{J}_c$ is reversed, the result remains the same [see Fig. 5(c)]. This shows that SOT loses control on the magnetic state and only H_{ext} is effective. We therefore treat this as an unsuccessful SOT

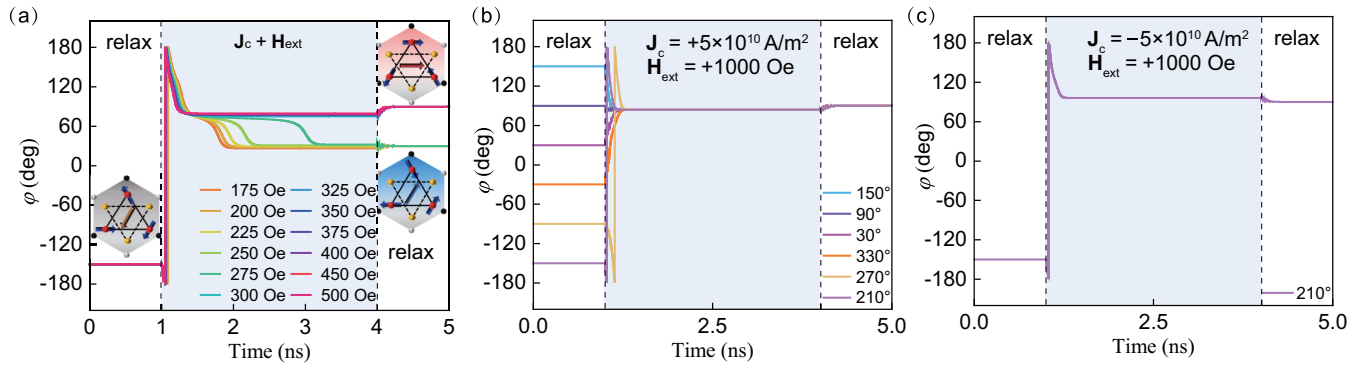

FIG. 5. (a) When $\mathbf{J}_c = +5\times10^{10}$ A/m^2, the dynamics of octupole moment under different H_{ext}. Starting from different initial states, the dynamics of octupole moment when (b) $\mathbf{J}_c = +5\times10^{10}$ A/m^2 and (c) $\mathbf{J}_c = -5\times10^{10}$ A/m^2 with $\mathbf{H}_{ext} = +1000$ Oe.

switching, which is illustrated in Fig. 3(e) as the light blue region.

In fact, the magnetization switching in configuration II has been experimentally observed recently [32]. However, the authors attributed it to the misalignment of crystalline orientation, and then explained the results using the switching mechanism in configuration I. Further experiments will be beneficial to clarify the underlying physics. Besides obtaining a high quality sample, we suggest that a phase diagram measurement, including sweeping $\mathbf{H}_{\text{ext}}$ and $\mathbf{J}_{\text{c}}$, would be helpful for a better understanding.

During the preparation of this manuscript, the experimental study of switching Mn_3Sn in configuration II was published [33], where the opposite switching polarity between Mn_3Sn and ferromagnets observed in our work was demonstrated experimentally, i.e., the handedness anomaly defined in their paper. However, to achieve the switching in their system, it requires the strain induced modification of exchange constant and anisotropy, especially the additional uniaxial anisotropy that points in the same direction for all the atoms. The additional anisotropy and the unequal exchange constant between sublattices may lead to the distortion of spin configuration [17] and further complicate the physical picture. In contrast, in our work, we propose a clean switching picture and demonstrate that these strain related modifications are not required, which can greatly simplify the device engineering.

IV. CONCLUSION

We have demonstrated deterministic SOT switching of Mn_3Sn in configuration II where the spin polarization is perpendicular to the kagome plane. We show that J_{crit} is in the order of 10^{10} A/m^2 and H_{ext} is around a hundred Oersted. We show that the switching result is uniquely determined by the combination of $\mathbf{J}_{\text{c}}$ and $\mathbf{H}_{\text{ext}}$. These properties are similar to the ferromagnet. However, the unique spin structure of Mn_3Sn also leads to distinct features. The switching relies on the balance of effective SOT field and $\mathbf{H}_{\text{ext}}$, based on which we verify that J_{crit} increases linearly with H_{ext}. In addition, the complex spin structure results in an opposite switching polarity compared to the ferromagnet. We conclude that the mechanism in ferromagnets cannot be directly applied to Mn_3Sn. Finally, we provide the switching phase diagram as a guideline for experimental demonstration.

The data that support the findings of this study are available from the corresponding author upon reasonable request.

ACKNOWLEDGMENTS

This work was supported by the National Key R&D Program of China (Grant No. 2022YFB4401700), National Natural Science Foundation of China (Grants No. 12104301 and No. 12104032), and Beijing Nova Program (Grant No. Z211100002121123).

[1] S. Shi *et al.*, All-electric magnetization switching and Dzyaloshinskii-Moriya interaction in WTe_2/ferromagnet heterostructures, Nat. Nanotechnol. **14**, 945 (2019).

[2] X. Wang *et al.*, Room temperature field-free switching of CoFeB/MgO heterostructure based on large-scale few-layer WTe_2, Cell Rep. Phys. Sci. **4**, 101468 (2023).

[3] J. Hong, K. Dong, J. Bokor, and L. You, Self-assembled single-digit nanometer memory cells, Appl. Phys. Lett. **113**, 062404 (2018).

[4] K. Garello, F. Yasin, S. Couet, L. Souriau, J. Swerts, S. Rao, S. V. Beek, W. Kim, E. Liu, S. Kundu, D. Tsvetanova, K. Croes, N. Jossart, E. Grimaldi, M. Baumgartner, D. Crotti, A. Fumemont, P. Gambardella, and G. S. Kar, SOT-MRAM 300MM integration for low power and ultrafast embedded memories, in *Proceedings of the 2018 IEEE Symposium on VLSI Circuits* (IEEE, New York, 2018), pp. 81–82.

[5] K. Fritz, L. Neumann, and M. Meinert, Ultralow switching-current density in all-amorphous W−Hf/Co−Fe−B/TaOx Films, Phys. Rev. Appl. **14**, 034047 (2020).

[6] B. Jinnai, J. Igarashi, K. Watanabe, T. Funatsu, H. Sato, S. Fukami, and H. Ohno, High-performance shape-anisotropy magnetic tunnel junctions down to 2.3 nm, in *Proceedings of the IEEE International Electron Devices Meeting (IEDM)* (IEEE, Piscataway, NJ, 2020), pp. 24.6.1–24.6.4.

[7] S. Hu *et al.*, Efficient perpendicular magnetization switching by a magnetic spin Hall effect in a noncollinear antiferromagnet, Nat. Commun. **13**, 4447 (2022).

[8] D. Meng *et al.*, Field-free spin-orbit torque driven perpendicular magnetization switching of ferrimagnetic layer based on non-collinear antiferromagnetic spin source, Adv. Electron. Mater. **10**, 2300665 (2024).

[9] C. Cao *et al.*, Anomalous spin current anisotropy in a noncollinear antiferromagnet, Nat. Commun. **14**, 5873 (2023).

[10] J. Lu *et al.*, Voltage-gated spin-orbit torque switching in IrMn-based perpendicular magnetic tunnel junctions, Appl. Phys. Lett. **122**, 012402 (2023).

[11] J. Železný, H. Gao, K. Výborný, J. Zemen, J. Mašek, A. Manchon, J. Wunderlich, J. Sinova, and T. Jungwirth, Relativistic Néel-order fields induced by electrical current in antiferromagnets, Phys. Rev. Lett. **113**, 157201 (2014).

[12] P. Wadley *et al.*, Electrical switching of an antiferromagnet, Science **351**, 587 (2016).

[13] Z. Xu, J. Ren, Z. Yuan, Y. Xin, X. Zhang, S. Shi, Y. Yang, and Z. Zhu, Field-free spin–orbit torque switching of an antiferromagnet with perpendicular Néel vector, J. Appl. Phys. **133**, 153904 (2023).

[14] X. Zhou, X. Chen, J. Zhang, F. Li, G. Shi, Y. Sun, M. Saleem, Y. You, F. Pan, and C. Song, From fieldlike torque to antidamping torque in antiferromagnetic Mn_2Au, Phys. Rev. Appl. **11**, 054030 (2019).

[15] T. Nagamiya, S. Tomiyoshi, and Y. Yamaguchi, Triangular spin configuration and weak ferromagnetism of Mn_3Sn and Mn_3Ge, Solid State Commun. **42**, 385 (1982).

[16] H. Xie, X. Chen, Q. Zhang, Z. Mu, X. Zhang, B. Yan, and Y. Wu, Magnetization switching in polycrystalline Mn_3Sn thin film induced by self-generated spin-polarized current, Nat. Commun. **13**, 5744 (2022).

[17] T. Higo *et al.*, Perpendicular full switching of chiral antiferromagnetic order by current, Nature (London) **607**, 474 (2022).

[18] G. Q. Yan *et al.*, Quantum sensing and imaging of spin–orbit-torque-driven spin dynamics in the non-collinear antiferromagnet Mn_3Sn, Adv. Mater. **34**, 2200327 (2022).

[19] X. Liu, D. Zhang, Y. Deng, N. Jiang, E. Zhang, C. Shen, K. Chang, and K. Wang, Tunable spin textures in a kagome antiferromagnetic semimetal via symmetry design, ACS Nano **18**, 1013 (2023).

[20] Y. Deng, X. Liu, Y. Chen, Z. Du, N. Jiang, C. Shen, E. Zhang, H. Zheng, H.-Z. Lu, and K. Wang, All-electrical switching of a topological non-collinear antiferromagnet at room temperature, Natl. Sci. Rev. **10**, nwac154 (2023).

[21] S. Nakatsuji, N. Kiyohara, and T. Higo, Large anomalous Hall effect in a non-collinear antiferromagnet at room temperature, Nature (London) **527**, 212 (2015).

[22] H. Tsai *et al.*, Electrical manipulation of a topological antiferromagnetic state, Nature (London) **580**, 608 (2020).

[23] H. Tsai, T. Higo, K. Kondou, A. Kobayashi, T. Nakano, K. Yakushiji, S. Miwa, Y. Otani, and S. Nakatsuji, Spin–orbit torque switching of the antiferromagnetic state in polycrystalline Mn_3Sn/Cu/heavy metal heterostructures, AIP Adv. **11**, 045110 (2021).

[24] Y. Deng, R. Li, and X. Liu, Thickness dependent anomalous Hall effect in noncollinear antiferromagnetic Mn_3Sn polycrystalline thin films, J. Alloys Compd. **874**, 159910 (2021).

[25] Z. Zheng *et al.*, Effective electrical manipulation of a topological antiferromagnet by orbital torques, Nat. Commun. **15**, 745 (2024).

[26] B. Pal *et al.*, Setting of the magnetic structure of chiral kagome antiferromagnets by a seeded spin-orbit torque, Sci. Adv. **8**, eabo5930 (2022).

[27] G. K. Krishnaswamy, G. Sala, B. Jacot, C.-H. Lambert, R. Schlitz, M. D. Rossell, P. Nöel, and P. Gambardella, Time-dependent multistate switching of topological antiferromagnetic order in Mn_3Sn, Phys. Rev. Appl. **18**, 024064 (2022).

[28] Y. Takeuchi, Y. Yamane, J.-Y. Yoon, R. Itoh, B. Jinnai, S. Kanai, J. Ieda, S. Fukami, and H. Ohno, Chiral-spin rotation of non-collinear antiferromagnet by spin–orbit torque, Nat. Mater. **20**, 1364 (2021).

[29] S. Hu, C. Zheng, W. Fan, and Y. Liu, Terahertz magnetic excitations in non-collinear antiferromagnetic Mn_3Pt: Atomistic-scale dynamical simulations, J. Magn. Magn. Mater. **588**, 171393 (2023).

[30] A. Shukla, S. Qian, and S. Rakheja, Order parameter dynamics in Mn_3Sn driven by DC and pulsed spin–orbit torques, APL Mater. **11**, 091110 (2023).

[31] A. Shukla, S. Qian, and S. Rakheja, Impact of strain on the SOT-driven dynamics of thin film Mn_3Sn, J. Appl. Phys. **135**, 123903 (2024).

[32] T. Xu, H. Bai, Y. Dong, L. Zhao, H.-A. Zhou, J. Zhang, X.-X. Zhang, and W. Jiang, Robust spin torque switching of noncollinear antiferromagnet Mn_3Sn, APL Mater. **11**, 071116 (2023).

[33] J.-Y. Yoon *et al.*, Handedness anomaly in a non-collinear antiferromagnet under spin–orbit torque, Nat. Mater. **22**, 1106 (2023).

[34] Z. Zhu, J. Deng, X. Fong, and G. Liang, Voltage-input spintronic oscillator based on competing effect for extended oscillation regions, J. Appl. Phys. **125**, 183902 (2019).

[35] Z. Zhu, K. Cai, J. Deng, V. P. K. Miriyala, H. Yang, X. Fong, and G. Liang, Electrical generation and detection of terahertz signal based on spin-wave emission from ferrimagnets, Phys. Rev. Appl. **13**, 034040 (2020).

[36] X. Zhang, B. Cai, J. Ren, Z. Yuan, Z. Xu, Y. Yang, G. Liang, and Z. Zhu, Spatially nonuniform oscillations in ferrimagnets based on an atomistic model, Phys. Rev. B **106**, 184419 (2022).

[37] See Supplemental Material at http://link.aps.org/supplemental/10.1103/PhysRevB.109.134433 for the extra details about the magnetic moment dynamics for configurations I and II, and the summary of switching cases under different initial states and conditions in configuration I. The Supplemental Material also contains Ref. [22].

[38] L. Liu, O. Lee, T. Gudmundsen, D. Ralph, and R. Buhrman, Current-induced switching of perpendicularly magnetized magnetic layers using spin torque from the spin Hall effect, Phys. Rev. Lett. **109**, 096602 (2012).

[39] H. Fujita, Field-free, spin-current control of magnetization in non-collinear chiral antiferromagnets, Phys. Status Solidi Rapid Res. Lett. **11**, 1600360 (2017).

[40] C. O. Avci *et al.*, Fieldlike and antidamping spin-orbit torques in as-grown and annealed Ta/CoFeB/MgO layers, Phys. Rev. B **89**, 214419 (2014).